AEGIS

Auroral Energy and Global Investigation of the Jovian System

Students: G. H. Blüthner, S. Bonetti, B. B. Bolduc, K. Caruana, L. Dall'Osto, J. Juul, V. Koßack, C. Maher, A. Ortega, J. Roney, G. L. Robin, J. Siehr, L. Stroud, K. Swoboda, J. B. Trencsenyi

Tutors: O. Dhuicque, L. Schulz

Abstract

AEGIS is a proposed dual spacecraft mission, investigating how moon-driven mass-loading impacts high-energy processes inside the magnetosphere of large planetary bodies. AEGIS's primary science objectives are to quantify how rotational energy is transported by magnetospheric currents and deposited in the ionosphere. And how variations in the plasma sheet and solar wind affect this process. The mission comprises two orbiting spacecraft: Equatorial (E) and Polar (P). These follow two elliptical orbits in approximately 2:1 resonance, allowing for simultaneous observations of the equatorial plasma sheet, solar wind conditions at the bow shock, and the polar aurora. Both spacecraft will measure in parallel the particle energy and density distributions, current systems, wave-particle interactions and bulk structure at their respective locations. The polar payload will further measure ultraviolet emissions, tracing energetic ions and electrons accelerated to the poles, and measure upper atmospheric energy deposition.

Both spacecraft would employ three-axis stabilisation and be powered by solar arrays. These spacecraft will connect Jupiter's changing plasma source environments, magnetospheric energy transport, and energy deposition to the upper atmosphere for the first time. These causal links are necessary for connecting the chain of energy input, transport, and dissipation in the giant planet magnetospheres, providing insight to Jupiter, its fellow giant planets in our solar system, and those in exoplanetary systems.

1 Introduction

Magnetised bodies in space influence their plasma environment and form a region named the magnetosphere. Within this region, the internal magnetic field imposed by the body controls the charged-particle motion over external influences such as the solar wind. This structure varies in dynamics, shape, plasma interactions, and extent, depending on magnetic moment, rotation rate, solar-wind conditions and plasma sources. Earth's magnetosphere acts as the archetype for magnetised rocky planets, while Jupiter hosts the most energetic magnetosphere in the Solar System [1]. The continuous stream of solar wind radially propagating from the Sun through the interplanetary plasma interacts with a planet's magnetic field. Where this interaction occurs, the 'bow shock' forms and supersonic plasma flow is decelerated, compressed, heated and deflected. Downstream of the bow shock, the heated and compressed solar-wind plasma flows through the 'magnetosheath' and is diverted around the 'magnetopause'. This is the boundary between solar wind plasma and planetary plasma, over which some exchange of mass, momentum, magnetic flux occurs and energy dissipation occurs. On the nightside of the planet, a 'magnetotail' can extend to many hundreds of the planet's radius, in the case of Jupiter, even extending to the orbit of Saturn [2]. How these planetary magnetospheres store, transport, transform and lose energy is intrinsically linked to plasma interactions, which are governed by particle dynamics and electric/magnetic field evolution.

For large planets like Jupiter, the basic components of Earth's magnetospheric structure are mostly consistent, but physically much larger and more energetic. However unlike Earth, Jupiter's energy is not mainly sourced by solar wind. Instead it is provided by the rapid planetary rotation. Also, Jupiter is tilted at about 10 degrees from its spin axis [1]. These features induce volcanic activity on its moon, Io, through tidal stress. In turn, Io produces approximately $1000\,\mathrm{kg\,s^{-1}}$ of material to the magnetosphere [3]. This material is ionised, and as the rapidly spinning magnetic field sweeps over the outgassed material, these ions are picked up, accelerated, and co-rotate with the magnetic field [4]. Strong electrodynamic interactions from this plasma rotation produce a strong electric current system. This impact extends beyond the local torus and forms the Jovian plasma sheet. Flux tubes, bundles of magnetic field lines that transport plasma along magnetic fields, connect this region to the polar regions[1]. This results in is the brightest aurora observed in the Solar System, a radiation environment of extreme intensity, and a unique set of coupled processes.

2 Science Motivation

Observations of Jupiter's aurora reveal multiple overlapping spatial and temporal features. At the poles, auroral "footprints" of ultraviolet emissions follow Io's orbit, where field lines connect the moon to the polar ionosphere and transport its outgassed and ionised material [5]. First observations of the aurora were made with the Voyager 1 spacecraft [6], and subsequent observations with ground-based instruments demonstrated this moon-aurora connection [5]. The main emissions in Jupiter's aurora are separated by electric current direction; Zone I corresponds to upward currents and Zone II to downward currents [7], though the exact driving mechanisms of precipitating particles in each zone are still not understood [8]. The brightest auroral emissions are thought to be caused by turbulent particle acceleration, but the energy profiles associated with these particles are broader than anticipated [9], and existing instruments have yet to measure far into the MeV energy range [10]. Some observational evidence has connected Zone I electron energy and density depletion to intense, short-period plasma waves at whistler mode frequencies ($<$10kHz) [11], while Zone II has been associated with large-amplitude solitary waves [10]. Additionally, snapshots from previous missions lack the required sampling rate to investigate the aurora as it varies over the order of minutes [8].

Energy deposition into Jupiter's upper atmosphere sustains a thermospheric temperature $\sim$700 K greater than solar heating alone can account for. Proposed theories on the cause for this include auroral particle precipitation [12], ion drag from magnetic field resistance [13], and frictional heating [14]. Compression and expansion of the magnetic field generated from solar wind pressures may contribute around 135 K to this thermospheric temperature increase, amplifying these plasma heating processes [15]. Recent mapping of H_3^+ emission has revealed a continuous temperature gradient extending from the auroral regions to the equator, indicating global redistribution instead of high-latitude confinement [16]. The mechanism enabling this transport, opposing the rotational barrier imposed by Coriolis forces and ion drag, remains unknown.

Solar wind constitutes the external driver of this system. Recently, Juno has provided direct evidence of relativistic electron acceleration ($>$1 MeV) upstream to Jupiter's bow shock [17]. Solar wind activity is therefore suspected to be an important factor in energetic processes in the Jupiter magnetosphere, but these interactions are not well constrained [18].

The dynamic and densely populated plasma torus structure is corotating with Jupiter up to around 20-40 Jupiter radii (RJ). After which, the plasma angular velocity drops, called the co-rotation breakdown [19]. The Hill-Cowley-Bunce model predicts that plasma originating at Io moves outwards along the plasma sheet, and by angular momentum conservation, lags progressively behind corotation. This lag imposes an azimuthal 'bending-back' on the magnetic field, causing radial currents in the equatorial plane that close in the ionosphere via field-aligned currents. The upward component of this current system is carried by downward-precipitating electrons, and this increase in momentum transfer accelerates electrons into Jupiter's ionosphere, which is thought to produce the main auroral emissions [20]. Observations have determined increased brightness in the aurora in tandem with increased Io activity and torus brightness [21].

These problems share a common obstacle of requiring simultaneous knowledge of driver (in equatorial plasma sheet) and consequence (in auroral ionosphere) yet every mission to date has comprised one spacecraft and has thus been unable to do this. The corotation breakdown cannot be linked directly to its energy deposition into the ionosphere. And the contribution to the dynamics of auroral heating cannot be pinned into torus-driven or solar-wind-driven components. Further, acceleration processes evolving in mere minutes cannot be resolved by a platform that samples each region once per orbit. AEGIS addresses this limitation directly, flying two spacecraft in near-perpendicular orbits to enable conjugate measurement of cause and effect, as we will now see by comparing to some heritage missions.

2.1 Heritage

Four missions define the current understanding of the Jovian magnetosphere. Galileo first encountered the system and gave us a broader overview. Juno (2016-present) carries a polar-orbiting suite of particle, field, and ultraviolet instruments, and established that broadband stochastic processes rather than quasi-static potentials dominate auroral energy delivery. JUICE (arriving 2031) will study the magnetosphere and its coupling to the Galilean moons, with improved fields and particles instrumentation, including vector electric-field measurement. Europa Clipper (arriving 2030) samples the plasma environment near 9-10 nR_J during its Europa flybys, though its focus is the moon rather than the magnetosphere.

2.2 Knowledge Gaps and Challenges

Decades of observations have attempted to uncover the mechanisms of energy transport in Jupiter's magnetosphere through a combination of ground-based, space-based, and in-situ observations. Existing missions have mostly observed individual regions, potentially inferring system links obtained non-simultaneously with other observatories [22, 23].

A principal uncertainty in this system is determining the role of corotation breakdown for driving the main aurora [24]. Current observations have not simultaneously observed the lag in plasma rotation, measuring plasma angular velocity, electron energy and density distributions, precipitating energy flux, wave measurements and UV emissions with sufficient temporal correlations to establish this pathway.

Similarly, the mechanisms and contributions of particle acceleration mechanisms are under debate. Juno has evidenced several processes, including quasi-static potentials, Alfvén waves, whistler scattering, and turbulence [23, 25, 26]. Determining what relative contributions each mechanism makes to the total auroral energy input is still an area of active research. Juno lacked simultaneous DC electric field measurements, leading to incomplete vector wave fields and preventing direct constraints between acceleration mechanisms [27].

An additional challenge for observing plasma population and atmospheric response is temporal variability. Internal plasma production and external solar wind forcing can vary on timescales from minutes to months [28]. Io's volcanic activity modifies the density and composition of the plasma sheet, while solar wind fluctuations act to compress or expand the magnetosphere. The primary method for inferring relationships between internal and external drivers to auroral activity has been combining observations from separate instruments or missions. Continuous and simultaneous observations monitoring these driving plasma populations with atmospheric responses are not yet viable.

The recent discovery of relativistic electrons upstream to Jupiter's bow shock demonstrates the importance of constraining these solar wind interactions to the Jovian system's energy balance [17]. Quantifying the frequency of these energetic events, as well as the transport of these particles into the system, requires more observations than intermittent bow shock crossings.

The common observational constraint of existing missions is the focus on independent parts of this complicated and interlinked system. The inner magnetosphere and auroral regions are observed independently of the outer magnetosphere and solar wind interactions. As a result, energy sources, transport mechanisms, and atmospheric responses are rarely reported under identical conditions. Without this, causal relationships and isolating internally driven variability from external disturbances are not yet accessible.

2.3 Scientific Objectives and Requirements

Addressing the outstanding questions surrounding Jupiter's energetic processes in its magnetosphere requires simultaneous measurements connecting causes and effects. This motivates a mission architecture of two complementary spacecrafts in near-resonant orbits, which can make parallel observations of physically connected regions of the Jovian system. The polar spacecraft would follow a high-inclination, highly elliptic orbit to investigate how the polar magnetospheric and auroral acceleration region responds to fluctuations in electric and magnetic fields, and precipitating particle energy and density distributions via the spatial and temporal ultraviolet auroral response. The second spacecraft, Equator, would establish how the energy sources in the equatorial magnetosphere plasma environment change, as well as how high-energy processes on the dayside affect the energy input to the system.

By operating simultaneously, these spacecraft will connect changing plasma source environments, transport through the magnetosphere, and deposition in the Jovian upper atmosphere for the first time. Such measurements would allow these internal and external driving forces to be quantified in a consistent framework. These causal links are necessary for connecting the chain of energy input, transport, and dissipation in the giant planet magnetospheres, providing insight to Jupiter, its fellow giant planets in our solar system, and those in further exoplanetary systems.

And therefore, our mission statement follows:

Investigate how moon-driven mass-loading impacts high-energy processes inside the magnetosphere of large planetary bodies

Three fundamental questions organise the AEGIS science case:

1. How is Jupiter's rotational energy transported by magnetospheric currents, and deposited in the ionosphere?
2. How do variations in the plasma sheet and solar-wind change the energy supplied to the Jovian magnetosphere?
3. How is solar-wind energy transformed across Jupiter's bow shock and transported into the magnetosphere?

From these (and the gaps identified above), four mission objectives follow:

- **M1.1** Determine if and how corotation breakdown, couples to the ionosphere via field-aligned currents, and its role in auroral energy deposition.
- **M1.2** Measure the fraction of the main aurora is powered by quasi-static potentials vs wave–particle processes.
- **M1.3** Quantify the dynamics of auroral heating during changing plasma torus and solar-wind conditions.
- **M1.4** Determine energy injection during changing solar wind conditions and relativistic electron accelerations at the planetary bow shock.

Each objective decomposes into science requirements, and hence into measurement requirements, and thus into instrument requirements.

3 Mission Design

The following sections describe the mission design. After the definition of the objectives and the subsequent mission and measurement requirement, a traceability matrix is created to keep track of the requirements driving the payload selection. Together with the concept of operation, a table which defined the operation mode of the spacecraft (which instrument is one and when) is created.

3.1 Mission Timeline

The proposed timeline breakdown of the AEGIS is shown in Table 1. Phases 0-D include all mission development on the science and engineering side. Phases E-F include mission launch, data collection and end-of-life operations, though an extension of the mission is possible through the fuel and radiation margins.

Table 1: Mission phases of AEGIS mission.

Phase	Amount of Time in Phase
Phase 0	2026 to 2029
Phase A	2029 to 2033
Phase B	2033 to 2035
Phase C/D	2035 to 2044
Phase E/F	2044 to 2052

AEGIS is a Category II mission, according to the debris mitigation and disposal classification system. Both spacecraft will perform a controlled atmospheric entry into Jupiter in the year 2052, after 2 years and 65 days of observations.

3.2 Trajectory and Orbit

The mission trajectory consists of two distinct phases. First, a heliocentric Earth-Venus-Earth-Earth-Jupiter (EVEEJ) gravity assist transfer, including Venus and Earth gravity-assist flybys, that delivers the spacecraft stack to the edge of Jupiter's sphere of influence (SOI). Then, a Jupiter system phase in which the two spacecraft separate and are independently targeted onto their respective science orbits. Both spacecraft share an identical incoming state at the SOI crossing. Separation is achieved through small impulsive burns applied at this large distance ($\sim$674 R_J) from Jupiter, which is less costly than performing the same manoeuvre close to the planet ($\Delta h = r \times \Delta v$). Polar spacecraft is targeted directly onto a near-polar capture orbit, while Equatorial spacecraft is directed toward a Callisto flyby, whose gravity assist reshapes the trajectory onto a low-inclination equatorial orbit at low propellant cost.

Upon reaching Jupiter, both spacecraft are propagated and targeted in GMAT to their respective final science orbits, summarised in Table 2. Figure 1 shows the resulting orbit geometry about Jupiter, together with the orbits of the Galilean moons used for the Callisto gravity assist.

Table 2: Jupiter orbit insertion with final orbits.

	Polar	Equatorial
Orbit Type	Polar	Equatorial
Periapsis	1.29 R_J	21.0 R_J
Apoapsis	99.4 R_J	101.0 R_J
Inclination	90°	4.1°
Period	28 days	58 days
Insertion Δv	1348.5 m/sec	1048.5 m/sec

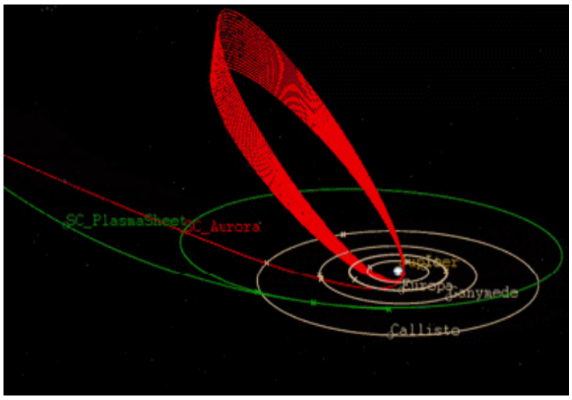

Figure 1: GMAT visualization of the Polar and Equatorial spacecraft orbits.

4 Spacecraft Design

The following sections describe the spacecraft design.

4.1 Payload

The mission will consist of two spacecraft flying in semi-perpendicular orbits. Polar and Equatorial will orbit at an inclination of 90° and at 4.1°, respectively. Each spacecraft will have a set of instruments vital to their mission objectives, listed in Table 3.

Table 3: Instrument suite identified per spacecraft

Instrument Name	Polar (P)/ Equatorial (E)
UVS Juice	P
UVI SMILE	P
REPT	P + E
Juno FGM	P + E
JEI JUICE	P + E
JDC JUICE	P + E
JoEE JUICE	P + E
JENI JUICE	E
RPWI LP-PWI & SCM	P + E

Each instrument was selected to perform a function related to the scientific objectives. The particle instruments are labelled together as PEEPIP and PEEPIE (Particle Environment Electron Proton Ion Polar/Equatorial).

UVS (Ultraviolet Spectrograph): This instrument will observe Jupiter's aurora and analyse the emission of UV light. It will map the aurora in Jupiter's upper atmosphere to characterise the spectral signatures.

UVI (Ultraviolet Imager) SMILE: This instrument is a UV auroral camera, employed on the polar spacecraft to study and map auroral activity.

REPT (Relativistic Electron-Proton Telescope): This instrument is a highly sensitive energetic particle spectrometer which will be used to study how the radiation particles are accelerated, transported and distributed around Jupiter's magnetosphere and aurora.

FGM (Fluxgate Magnetometer): The magnetometer takes 3D measurements of Jupiter's magnetic field to measure its strength and direction and will map Jupiter's magnetospheric and investigate interactions with the solar winds, plasma waves and turbulence [29].

JEI (Jovian Electron and Ion): The JEI is a sensor that will measure the distribution density and energy of electrons and ions in the magnetosphere and plasma environments.

JDC (Jovian Dynamics and Composition Analyzer): This instrument is a 3D mass spectrometer that will study Jupiter's magnetosphere by observing the mass, energy and direction of ions and electrons.

JoEE (Jovian Energetic Electrons): This instrument is an electron particle spectrometer that will capture 3D measurements of electrons within the magnetosphere.

JENI (Jovian Energetic Neutrals and Ions): Detects ENAs and the loss and gain of energetic ions and the dynamics of plasma.

RPWI (Search Coil Magnetometer): This instrument will characterize the plasma, in addition to the magnetic and electric fields.

4.2 Structure

The structure subsystem contains the sizing for both spacecraft. The main design driver of the subsystem is the launcher and the overall mass of both spacecraft. The primary requirements can be listed as follows:

- The system must survive the stress generated during launch, in addition to the loads generated from the subsequent orbital manoeuvres.
- The system must fit inside the fairing of Ariane 64 and connect to the structural interface thereof.
- The total mass of the spacecraft, including propellant, must be equal to, or lower than, the maximum allowable mass given by the launcher performance and target orbits.

Based on these initial top-level requirements, the initial allocated mass of the whole spacecraft (the sum of Polar and Equatorial) can be approximated to 5800 kg. For initial sizing purposes, 20% of the total spacecraft mass was allocated to the structural subsystem.

For preliminary sizing purposes, the satellite is assumed to be monocoque, with no longitudinal or ring stiffeners, and with constant stiffness.

The spacecraft's thickness and materials are the principal contributors to the mass estimation. Al7075 is selected as the material from space flight heritage due to its optimal weight/performance ratio. The structure must withstand the axial and lateral loads generated by the launcher. Thickness is thus sized to be rigid from the natural frequencies of the launcher, as well as for tensile and compressive strength. A 20% of margin is applied to this number due to the assumptions made about the analysis.

4.3 Propulsion

A liquid bi-propellant propulsion system was selected for both spacecraft to meet the defined scientific requirements and Δv budget. Monomethylhydrazine (MMH) and nitrogen tetroxide (NTO) were selected as the fuel and oxidiser, respectively, providing a specific impulse of 350 s. An oxidiser-to-fuel (O/F) mass ratio of 1.64 was selected to achieve approximately equal-sized fuel and oxidiser tanks, thereby simplifying the structural design. The propulsion system employs an ArianeGroup 400 N-class main engine for orbit insertion, orbit maintenance and end-of-life disposal. This is complemented by four 22 N-class thrusters, which provide the fine control required for smaller manoeuvres, including launcher injection error correction. Attitude control is achieved using reaction wheels, with de-saturation performed by sixteen helium-fed cold-gas thrusters. The propellant is stored in tanks with capacities of 350 L (Polar) and 250 L (Equatorial), respectively, each pressurised to 25 bar. Pressurisation of these propellant tanks is provided by three 130 L helium tanks, which also supply the cold-gas thrusters. The mass and volume of the propellant and pressurant are summarised in Table 4, and the masses, volumes and dimensions of the propulsion system tanks are displayed in Table 5.

Table 4: Propellant and pressurant for both spacecraft.

	Polar	Equatorial
MMH (fuel)		
Mass (kg)	273	203
Volume (L)	312	232
NTO (oxidizer)		
Mass (kg)	450	333
Volume (L)	312	232
Helium (pressurant)		
Mass (kg)	1.16	0.96
Volume (L)	350	293

Table 5: Propellant and pressurant tanks for both spacecraft.

	Polar	Equatorial
MMH/NTO tank		
Mass (kg)	14	12
Volume (L)	350	250
Radius (m)	0.43	0.39
Thickness (mm)	1.15	1.08
Helium tank ($\times$3)		
Mass (kg, each)	4.7	3.9
Volume (L, each)	130	106
Radius (m)	0.31	0.29
Thickness (mm)	0.70	0.60

4.4 Electrical Power System

The Electrical Power System (EPS) has been characterised and sized according to the operational modes defined for each spacecraft. These operational modes satisfy the mission power requirements throughout their operational lifetime. The EPS architecture consists of three main elements: the solar array for power generation, the battery for energy storage, and the Power Control and Distribution Unit (PCDU) for power regulation and distribution.

During sunlit periods, both spacecraft are powered by the solar array, while the battery provides the required energy during eclipse periods. Therefore, the solar array sizing considers not only the instantaneous spacecraft power demand, but also the capability to recharge the battery during the available sunlight period before the next eclipse.

The power profile of each spacecraft derived from the defined operational modes provided the average orbital power consumption and peak instantaneous power demand. These values, together with the solar flux at Jupiter, the eclipse duration, the mission lifetime, and the degradation of the solar cells, were used to size the EPS in terms of power generation, energy storage, and total mass. A 20% design margin has been applied to the overall power budget to account for design uncertainties.

The selected solar cell is the AZUR SPACE 3G28 triple-junction GaAs cell, following the approach adopted by the Juno mission; the only solar-powered spacecraft to have successfully operated at Jupiter's heliocentric distance. The battery is based on the Saft VES180SA lithium-ion cell, selected due to its high specific energy and established space heritage. A regulated 28 V DC bus has been assumed, consistent with typical deep-space PCDU architectures. Table 6 summarizes the main EPS sizing parameters for both spacecraft.

Table 6: Power systems needed to generate sufficient power for the mission. SA*:solar array and BC*: battery capacity, BCC*: Battery cells configuration, DR*: Degradation rate.

Parameter	Polar	Equatorial
Ave. P_{req}	704.99 W	411.5 W
Peak P_{req}	854.81 W	658.19 W
SA* BOL P	1,048.74 W	614.94 W
SA* EOL P	1,005.77 W	589.75 W
SA* A	113.2 m^2	66.38 m^2
SA* M	97.35 kg	57.08 kg
Eclipse Dur.	8.47 h	16.16 h
BC*	14,256 Wh	15,552 Wh
Battery Mass	83.86 kg	91.48 kg

The difference in EPS sizing between both spacecraft is driven by their distinct operational requirements and orbital environments. Equatorial requires a smaller solar array due to its lower average power demand, while the Polar spacecraft requires a larger generation system to support its higher payload consumption. Conversely, the longer eclipse duration of the equatorial orbit (16.16 h compared with 8.47 h) drives a larger battery capacity, despite its lower average power consumption. In both cases, the EOL solar array power remains above the required operational demand, ensuring sufficient energy availability throughout the mission lifetime, while accounting for solar cell degradation and the reduced solar irradiance at Jupiter.

The PCDU mass and power consumption have been included in mass and power budgets. A 5% power consumption has been assumed for the PCDU to account for conversion and distribution losses, together with the associated harness contribution. This approach provides a consistent and conservative EPS sizing for both spacecraft.

4.5 Attitude Determination Control System (ADCS)

The Attitude Determination and Control Subsystem (ADCS) was sized based on the pointing requirements. The primary design driver is the pointing accuracy requirement of 0.1° during science observations, and during downlink operations.

To achieve this, both spacecraft are equipped with two star trackers, mounted on opposite sides of the spacecraft to ensure continuous attitude knowledge and provide redundancy in case of temporary sensor outages or obstructions. For coarse attitude determination, the ADCS additionally employs Sun sensors and an Inertial Measurement Unit (IMU).

Attitude control and spacecraft stabilization are performed using four reaction wheels arranged in a tetrahedral configuration. This configuration provides full three-axis control while maintaining redundancy in the event of a single wheel failure. The selected reaction wheels are HR12 units from Honeywell, providing a maximum momentum storage capacity of 50 Nms. Due to external disturbance torques (e.g. gravity gradient and solar wind pressure), the reaction wheels accumulate angular momentum as they operate. This is periodically removed through momentum de-saturation using 16 cold-gas thrusters, each producing 0.5 N.

4.6 Thermal Control System

The preliminary sizing of a spacecraft thermal control system (TCS) relies on two important edge cases: the worst case hot (WCH) and the worst case cold (WCC). For AEGIS, these respectively occur during the Venus flyby and while the spacecraft is in Jupiter's eclipse. For preliminary sizing purposes, the following assumptions were made:

- The spacecraft is operating at steady-state
- The spacecraft's bus is operating as a black box

- The spacecraft's internal temperature range is bound by the minimum and maximum operational temperatures of the most sensitive instrument found on board. This range is from -5^{o}C to 30^{o}C.

The WCH environment can first be used to compute the size of the radiator necessary to dissipate the excess heat. The following sources of heat were considered: radiative heat from the surrounding environment, environmental fluxes (sun flux, albedo flux, and infrared (IR) flux), internal heat generation, and radiator heat dissipation. Performing the thermal equilibrium with the help of these sources yields the following radiator area: 2.2 m^2 (combined spacecraft configuration) and 1.1 m^2 (per spacecraft for separated configuration). Maximising radiator heat dissipation with white paint ($\alpha = 0.1$ and $\epsilon = 0.85$) and protecting the bus with white beta cloth MLI coating ensures the spacecraft's survival capability in WCH.

The next step in TCS sizing required the consideration of WCC and whether active heating was necessary. This case, being subject to a much harsher, colder environment, experiences the following heat sources: environmental fluxes (IR flux), internal heat generation, radiator heat dissipation, and bus radiative heat loss. Given the environment of Jupiter's eclipse, minimising heat loss from the spacecraft bus was necessary. As such, bimetallic louvres were included in the design. This allowed the radiator emissivity to greatly reduce depending on the spacecraft's environment (going from $\epsilon_{Venus} = 0.85$ to $\epsilon_{Jupiter} = 0.15$). However, this reduction in heat emissivity was not sufficient to maintain the spacecraft above its minimum operational temperature of -5^oC. Thermal equilibrium found that a heater dissipating 85 W was needed for WCC survival.

Finally, internal heat dissipation and instrument cryocooling needed to be considered. While no internal heat transfer calculations were done at this stage, the inclusion of thermal straps and a cryocooler is needed.

4.7 Communications

Both spacecraft communicate directly with Earth, so no inter-satellite relay is required. Each carries a X/Ka-band suite comprising of a 2.5 m high-gain antenna for nominal downlink, a 0.5 m medium-gain antenna for cruise and contingency, and a 0.2 m low-gain antenna for safe mode. Downlink will use Ka-band (32 GHz) while X-band is retained for uplink, ranging, cruise operations and safe mode. Supporting equipment comprises the X/Ka-band amplifier, the transponder, and RF electronics including switches, filters and cabling.

At fixed aperture, the change from X- to Ka-band yields approximately 12 dB. The proposed transmitter is a variable-power travelling-wave-tube amplifier (54-144 W RF), presumably best operated adaptively such that output is reduced near opposition, where link margin is more plentiful, and raised toward maximum range.

During transmission, the high-gain antenna is Earth-facing, while the scientific instruments, including the booms, are located at the opposite side of the spacecraft to avoid communication interference. The Ka-band beam is approximately 0.26° wide, such that anti-Earth boom placement keeps them away from the beam axis such that the antenna blockage should be zero. The same separation isolates the magnetometer from the radio-frequency chain.

Approximate contact windows are computed for both spacecrafts against ESA's New Norcia (DSA 1), Cebreros (DSA 2) and Malargüe (DSA 3), over a representative 60-day interval following Jupiter orbit insertion.

The resulting downlink rate is $0.85\,\mathrm{Mbit\,s^{-1}}$. This number was obtained by an assumed lossless 2-ratio reduction by applying compression when possible (for the given noted instruments). The data is to be downlinked for 12h/day during downlink windows, accounting for ground station availability. The data budget and the resulting needed transmit days per orbit can be seen in Table 7.

Table 7: Data budget for both spacecraft. DL*: Downlink.

	P	E
Requirement	600 Gbit/orbit	250 Gbit/orbit
After Comp.	450 Gbit/orbit	190 Gbit/orbit
Avg. Downlink Window	16 days	15 days
Worst Case DL* Window	15 days	4 days
Needed Transmit Days	**12 days**	**5 days**

4.8 Onboard Computer (OBC) and Data Handling

The spacecraft is equipped with two redundant onboard computers to ensure reliable operations and fault tolerance. Each spacecraft computer incorporates two microprocessors, providing additional redundancy in the event of a processor failure.

The data handling system includes two redundant storage units to prevent data loss and ensure continuous operations. The total storage capacity of 256 GB was selected based on the worst-case downlink scenario per orbit. During periods with limited communication opportunities, caused by eclipse phases and reduced ground station visibility windows, the acquired data can be temporarily stored on board and transmitted during the following orbit. This ensures that all generated data can be retained until a suitable downlink opportunity is available.

5 Budget

5.1 Mass Budget

Table 8 displays the mass budget for both spacecraft. Mass margins were applied to the scientific payload based on TRL between 15-20%. An additional 20% system margin has been applied to each subsystem.

Table 8: Mass budget for both spacecrafts.

Subsystem	P Mass (kg)	E Mass (kg)
Payload	82	59
Structure and Mech.	1349	1350
Thermal	28	21
Power	200	162
Data Handling	80	80
AOCS	43	43
Propulsion	900	650
Total	**2682**	**2365**
Total combined	**5047**	

5.2 Power Budget

This breakdown balances the electrical consumption of the active subsystems against the constraints of solar cell degradation and low-illumination efficiency far from the Sun. Each component has a 5% margin added and then the total has an extra 20% margin

Table 9: Power budgets per spacecraft.

Category	Power (W) P	Power (W) E
Payload	83	44
Thermal	346	166
Power	27	16
Data Handling	61	61
AOCS	41	41
Propulsion	11	11
Total Cost	**569**	**339**
Total w/ Margin	**717**	**428**

5.3 Cost Breakdown

Table 10: Cost budget breakdown for both spacecraft, where payload cost is combined.

Category	Cost M €
ESA Payload Contribution	30
spacecraft 1 Development	500
spacecraft 2 Development	300
Industrial Costs (0.25×)	210
Mission & Science Operations	150
Contingency Margin (20%)	200
Launcher (Ariane 64)	135
Total Cost	**1525**

Table 10 shows a top-down estimate of the mission's overall costs. This high-level structure incorporates industrial overhead and concerns, launch logistics and operational margins along with actual physical components as to establish a realistic fiscal prediction at this stage of proposal maturity.

6 Ground Segment and Operations

AEGIS uses the ESA ESTRACK deep-space network, comprising the 35 m antennas at New Norcia, Cebreros and Malargue. These are spaced approximately 120° apart in longitude, providing near-continuous coverage of a deep-space target as the Earth rotates.

Rudimentary visibility analysis yielded contact windows for all three stations over a representative 60-day interval following Jupiter orbit insertion. Naive summation of the per-station totals is not physically meaningful as the station view periods overlap, and simultaneous coverage is counted twice. Merging overlapping intervals yielded availability in conjunction with shared visibility constraints. Both orbit Jupiter, so they occupy the same direction on the sky as seen from Earth to within a small fraction of antenna beamwidth.

Two allocation strategies were assessed. Time-sharing each antenna equally yielded roughly 12 hours per day per spacecraft. Dedicating whole stations yielded a better result, and so a dedicated assignment is to be adopted as the baseline.

The Sun-Earth-probe (SEP) angle governs link availability independently of geometry. When Jupiter approaches solar conjunction, solar plasma along the line of sight degrades the link beyond usability and no science downlink is scheduled. Because the SEP angle evolves at approximately 0.85° per day, outages would be predictable.

Mission operations will be done from the ESA ESOC in Darmstadt. The science data that is downlinked will be forwarded to the ESA science operations center ESAC, in Spain.

7 Launch Vehicle Selection

Ariane 64 was selected as the launch vehicle for this mission. The key drivers behind this choice are summarised below.

- **Escape-energy performance.** The EVEEJ transfer to Jupiter requires a departure characteristic energy of $C_3 \approx 9.4\ \mathrm{km^2\,s^{-2}}$ ($v_\infty \approx 3.06\ \mathrm{km\,s^{-1}}$). Ariane 64, flying with its four P120C solid boosters and a two-burn (ULPM double-burn) upper-stage strategy, is rated for exactly this class of escape mission and delivers an interpolated payload capability of ∼5.9 t at our required C_3 and launch asymptote declination (DLA ≈ 2.8°), comfortably in excess of the combined dry mass of both spacecraft.

- **Heavy lift dual manifest capability.** Carrying two independent spacecraft to Jupiter as a single co-manifested stack requires substantial injected mass margin; Ariane 64 is the highest-performance member of the Ariane 6 family and is sized for exactly this class of dual/heavy payload.

- **Flight heritage and reliability.** As the current flagship European launch vehicle, Ariane 64 benefits from a mature, ESA/ArianeSpace qualified design lineage, reducing programmatic and technical risk relative to a newer or less flown vehicle.

The sufficient escape mission payload margin at the mission's actual departure energy and declination, heavy-lift dual-payload capacity, and proven European launch heritage make Ariane 64 the natural choice of launch vehicle for this concept.

8 Concept of Operations

Operations are organised around four modes, selected according to orbital position and mission phase; Cruise mode, Science/Measurement mode, Downlink mode, Safe mode. The near-2:1 orbital resonance between the two spacecraft is exploited operationally to observe periods when the equatorial spacecraft samples a field line whose footprint is simultaneously visible to the polar spacecraft.

9 Mission Drivers

In transit between Earth and Jupiter, there are many different types of radiation that the spacecraft will experience with energies up to GeV that can damage the instruments. These are determined primarily by solar energetic particles (SEPs) and galactic cosmic rays (GCRs), eGCR, solar wind and the phases of the solar cycle [30, 31]. Trapped relativistic electrons in the inner magnetosphere produce total ionizing doses.

Dose was assessed using SPENVIS with the JOSE Jovian electron model, integrated over the mission trajectory. Behind 8 mm of aluminium-equivalent shielding, the total ionizing dose is approximately 144 krad for Polar and 44 krad for Equatorial, including a factor-of-two radiation design margin. The difference follows directly from orbit geometry, and mitigation follows the approach demonstrated by Juno. The JOSE model calculates fluxes in the Jovian magnetosphere for 5 species: electron, proton, carbon, oxygen and sulphur.

Another mission driver is thermal protection, which will dictate active heating and cooling systems as some of our instruments require specific temperature ranges.

10 Risk Assessment

Evaluating the risk profile of this dual spacecraft mission requires balancing extreme environmental hazards with operational complexities introduced by the stipulated requirements and worsened by multi-vehicle coordination. The Jovian environment presents challenges due to intense radiation belts and solar energy limitations. The following matrix in Fig. 2 establishes a framework for engineering margins, hardware redundancies and general safeguards.

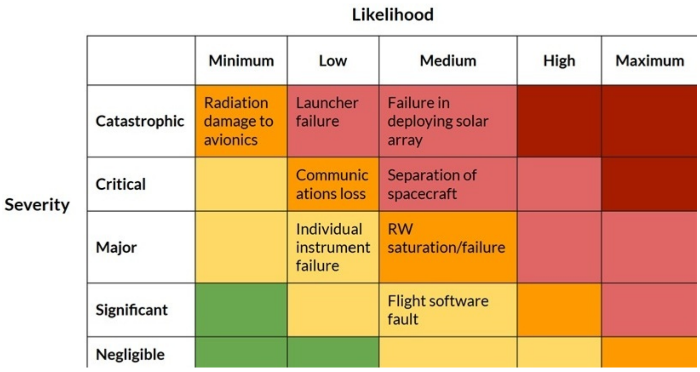

Figure 2: Risk Assessment Matrix for the space mission that shows the likelihood a risk will occur and the severity of its impact.

11 Technological Readiness Level TRL

All the instruments on board have been proven flight ready by heritage space missions such as JUNO, JUICE, SMILE and RBSP but have to be adapted to the specific environments that they will be exposed to during the mission lifetime. Table 11 shows the TRL of each instrument aboard the mission.

Table 11: Technological Readiness Level of each instrument aboard the Polar and Equatorial spacecrafts.

Instrument	TRL	Instrument	TRL
UVS	7	JoEE	6
UVI	7	JENI	6
REPT	5	RPWI	6
FGM	8	JDC	6
JEI	6		

12 Conclusion

AEGIS will observe how the Jovian magnetosphere stores, transports, transforms, and deposits energy. These processes, linking the particle and field dynamics of the plasma sheet, solar wind, aurora, and, will be observed simultaneously for the first time using a dual-spacecraft architecture in near-2:1 orbital resonance. The polar payload outlined will measure energy deposition to the upper atmosphere, in parallel with the equatorial craft measuring the bulk plasma properties, particle acceleration, current-system closure, and wave-particle interaction. The unique measurement geometry means we can link processes occurring at different locations for the first time. We will gain insight into connected processes of particle interactions, magnetic fields and wave interactions in the Jovian system, enhancing our knowledge of these high-energy processes. This project bridges the gap no single-spacecraft mission has been able to address, a limit of heritage missions like Juno.

AEGIS offers the prospect of properly determining how rapidly rotating magnetised systems process and dissipate energy, with implications extending from Saturn and other giant planets, to magnetised exoplanets, and to the habitability of the environments they host.

In line with the science objectives, this report highlighted the preliminary sizing of the mission's subsystems. While many assumptions were made, the subsystems proved to be feasible and worthy of further exploration in a future, more in depth study.

13 Acknowledgement

The Red Team expresses sincere gratitude to FFG, ESA and Austrospace for organising the Alpbach Summer School 2026. We thank the tutors for their guidance and support throughout. Special thanks to our engineering tutor, **O. Dhuicque**, for her technical insights, and to our science tutor, **L. Schulz**, for his scientific expertise and mentorship.

References

[1] F. Bagenal. In: *Planets, stars and stellar systems* (2013), p. 251.

[2] Krishan K Khurana et al. In: *Jupiter. The planet, satellites and magnetosphere* 1 (2004), pp. 593–616.

[3] Roth L. et al. In: *Space Sci Rev* 221 (2025). URL: https://doi.org/10.1007/s11214-025-01137-x.

[4] D.D. Barbosa et al. In: *Geophysical Research Letters* (1983), pp. 593–616.

[5] John T Clarke et al. In: *Science* 274.5286 (1996), pp. 404–409.

[6] John T Clarke et al. In: *Jupiter: The planet, satellites and magnetosphere* 1 (2004), pp. 639–670.

[7] B. Mauk et al. In: *Journal of Geophysical Research: Space Physics* 125.3 (2020). URL: https://agupubs.onlinelibrary.wiley.com/doi/abs/10.1029/2019JA027699.

[8] L. Fletcher et al. In: *Space Science Reviews* 219.7 (2023). URL: http://dx.doi.org/10.1007/s11214-023-00996-6.

[9] F. Allegrini and otherse. In: *Journal of Geophysical Research: Space Physics* 125.4 (2020).

[10] A. H. Sulaiman et al. In: *Journal of Geophysical Research: Space Physics* 127.8 (2022). URL: https://agupubs.onlinelibrary.wiley.com/doi/abs/10.1029/2022JA030334.

[11] Kurth et al. In: *Geophysical Research Letters* 45.18 (2018). URL: https://agupubs.onlinelibrary.wiley.com/doi/abs/10.1029/2018GL078566.

[12] Grodent et al. In: *Journal of Geophysical Research: Space Physics* 106.A7 (2001), pp. 12933–12952.

[13] George Millward et al. In: *Icarus* 173.1 (2005), pp. 200–211.

[14] Aharon Eviatar and David D Barbosa. In: *Journal of Geophysical Research: Space Physics* 89.A9 (1984), pp. 7393–7398.

[15] Japheth N Yates, Nick Achilleos, and Patrick Guio. In: *Planetary and Space Science* 61.1 (2012), pp. 15–31.

[16] J. O'Donoghue et al. In: *Nature* 596 (2021). URL: https://doi.org/10.1038/s41586-021-03706-w.

[17] Raptis S. et al. In: *Nature* 654 (2026).

[18] M. J. Rutala et al. In: *Journal of Geophysical Research: Space Physics* 130.5 (2025). URL: https://agupubs.onlinelibrary.wiley.com/doi/abs/10.1029/2025JA033842.

[19] Pontius Jr et al. In: *Geophysical Research Letters* 9.12 (1982).

[20] Head, L. A. et al. In: *AA* (2024). URL: https://doi.org/10.1051/0004-6361/202450253.

[21] Chihiro Tao et al. In: *Geophysical Research Letters* 45.1 (2018). URL: https://agupubs.onlinelibrary.wiley.com/doi/abs/10.1002/2017GL075814.

[22] J.D. Nichols et al. In: *Geophysical Research Letters* 50.20 (2023), e2023GL105549.

[23] D-X. Pan et al. In: *Geophysical Research Letters* 48.5 (2021).

[24] A. Groulard et al. In: *Icarus* (2024). URL: https://www.sciencedirect.com/science/article/pii/S0019103524000630.

[25] CTS Lorch et al. In: *Journal of Geophysical Research: Space Physics* 127.6 (2022).

[26] NK Dwivedi et al. In: *Physica Scripta* 99.4 (2024), p. 045028.

[27] A Salveter et al. In: *Journal of Geophysical Research: Space Physics* 130.7 (2025).

[28] J-Z. Wang et al. In: *Geophysical Research Letters* (2026). DOI: 10.1029/2026GL123313.

[29] JEP Connerney et al. In: *Space Science Reviews* 213.1 (2017), pp. 39–138.

[30] W. Hajdas et al. "The JUICE Radiation Environment Monitor, RADEM". In: *Space Science Review* 221 (2025).

[31] Pinto, M. et al. In: *AA* 708 (2026), p. 43. URL: https://doi.org/10.1051/0004-6361/202558601.